Nanoscale

RSC Publishing

PAPER

View Article Online
View Journal | View Issue

Cite this: *Nanoscale*, 2013, **5**, 10236

Direct observation of rotatable uncompensated spins in the exchange bias system Co/CoO–MgO

Chuannan Ge,[ab] Xiangang Wan,*[a] Eric Pellegrin,*[c] Zhiwei Hu,[d] S. Manuel Valvidares,[c] Alessandro Barla,[ce] Wen-I. Liang,[f] Ying-Hao Chu,[f] Wenqin Zou[a] and Youwei Du[a]

Received 23rd April 2013
Accepted 27th July 2013

DOI: 10.1039/c3nr02013d

www.rsc.org/nanoscale

We have observed a large exchange bias field $H_E \approx 2460$ Oe and a large coercive field $H_C \approx 6200$ Oe at $T = 2$ K for Co/CoO core–shell nanoparticles (~4 nm diameter Co metal core and CoO shell with ~1 nm thickness) embedded in a non-magnetic MgO matrix. Our results are in sharp contrast to the small exchange bias and coercive field in the case of a non-magnetic Al_2O_3 or C matrix materials reported in previous studies. Using soft X-ray magnetic circular dichroism at the Co-$L_{2,3}$ edge, we have observed a ferromagnetic signal originating from the antiferromagnetic CoO shell. This gives direct evidence for the existence of rotatable interfacial uncompensated Co spins in the nominally antiferromagnetic CoO shell, thus supporting the uncompensated spin model as a microscopic description of the exchange bias mechanism.

1 Introduction

Exchange bias (EB) was first reported by Meiklejohn and Bean in the system of partially oxidized Co particles.[1] The outstanding characteristic of EB is a hysteresis loop shifting with the magnetic field, which is commonly accompanied with an increase of coercivity (H_C) and the appearance of a unidirectional anisotropy. EB has already been widely used in magnetoresistive reading heads,[2,3] as well as spin valve-based devices,[4] and has also been proposed as an efficient way to stabilize the written information against thermal fluctuations in magnetic recording media.[5] Although tremendous efforts have been devoted to understand this intriguing phenomenon and to find out new systems for various applications,[6–14] the microscopic origin of the EB effect is still controversially discussed in terms of uncompensated interfacial spins,[13–15] spin flop-coupling within the ferromagnetic (FM) and antiferromagnetic (AFM) layers,[16,17] and spin canting within the AFM system induced by the exchange coupling between the FM and the AFM layers.[5] The generally accepted uncompensated spin scenario can reasonably well explain the EB due to the existence of pinned uncompensated spins as well as the enhanced coercive field due to the existence of rotatable uncompensated spins at the interface.[15,26]

It was found that the Co/CoO core–shell system has a larger exchange bias field (H_E) than the Co/CoO bilayer system.[5] This has been previously interpreted as a consequence of an increase of the surface-to-volume ratio and of the interface roughness between the Co core and the CoO shell.[18] The associated uncompensated interfacial spins are not easy to measure directly,[19] thus a precise experimental analysis of the microscopic origin of EB is still lacking.

In this work, we have studied a series of Co/CoO core/shell nanoparticles embedded in a MgO matrix, considering that this core/shell system has several interesting aspects:[5] (a) a high exchange field and a high coercive field, (b) the stabilization of not only the ferromagnetism of the Co core cluster but also the antiferromagnetism of the CoO core shell, and (c) the magnitude of the EB that can be correctly estimated by theory. In contrast to Co/CoO core/shell nanoparticles in a non-magnetic Al_2O_3 matrix,[5] in this work we could observe a large exchange bias and a large coercive field for the same kind of nanoparticles embedded in equally non-magnetic MgO. Moreover, using X-ray magnetic circular dichroism (XMCD) at the Co-$L_{2,3}$ edges, we have observed a sizeable FM signal from the AFM CoO shell, which cannot be assigned to the canted AFM spins of the polycrystalline Co/CoO core–shell systems due to the large magnetic anisotropy energy of the Co^{2+} ion.

2 Experimental

A series of Co/CoO–MgO (CCMO) granular films were deposited on Si(100) substrates by magnetron sputtering in an oxygen

[a]*National Laboratory of Solid State Microstructures and Department of Physics, Nanjing University, Nanjing 210093, China. E-mail: xgwan@nju.edu.cn*

[b]*Department of Physics, Jiangsu Institute of Education, Nanjing 210013, China*

[c]*CELLS-ALBA Synchrotron Radiation Facility, Carretera BP 1413, km 3.3, E-08290 Cerdanyola del Vallès, Barcelona, Spain. E-mail: epellegrin@cells.es*

[d]*Max Planck Institute for Chemical Physics of Solids, Nöthnitzer Straße 40, D-01187 Dresden, Germany*

[e]*Istituto di Struttura della Materia, ISM CNR, S.S. 14 km 163.5, Area Science Park Basovizza (Ts), Trieste I-34149, Italy*

[f]*Department of Materials Science and Engineering, National Chiao Tung University, Hsinchu 30010, Taiwan*

partial pressure of 2×10^{-7} mbar using a RF power of 140 W and a typical deposition time of one hour. The sputtering targets were mosaic-like, made by adhering small square-shaped pieces of highly purified cobalt metal onto a MgO plate. Thus, the ratio of Co metal to the MgO surface on the target determined the resulting Co atomic composition ratio. All Co/CoO–MgO granular films were prepared at room temperature. During the sputtering process Co atoms form metallic clusters that are oxidized in the oxygen atmosphere, thus resulting in the formation of thin CoO shells. The exact composition of all samples was investigated by energy dispersive X-ray spectroscopy (EDX). The resistance of all samples was measured using the four-terminal measuring technique and their magnetic characterization was performed using a Quantum Design SQUID magnetometer.

The X-ray magnetic circular dichroism (XMCD) spectra at the Co-$L_{2,3}$ edges were collected at the BL29 Boreas beamline at the CELLS-ALBA synchrotron radiation facility (Barcelona, Spain) with a photon energy resolution of 0.25 eV and a degree of circular polarization close to 100% in a magnetic field of 5 Tesla and at a sample temperature of 80 K. The spectra were recorded using the total electron yield method (by measuring the sample drain current) in a chamber with a vacuum base pressure of 2×10^{-10} mbar.

3 Results and analysis

The morphology of the Co/CoO core–shell systems embedded in a nonmagnetic MgO matrix was revealed by high-resolution transmission electron microscopy (HRTEM). Fig. 1(a) and (b) show typical HRTEM images of the $Co_{69}Mg_7O_{24}$ and the $Co_{80}Mg_6O_{14}$ sample (called CCMO1 and CCMO2 hereafter), where small Co clusters covered with a CoO shell embedded in a MgO matrix can be observed. The mean diameter of the Co clusters and the thickness of the CoO shell are of the order of 4–5 nm and 1–2 nm, respectively. The sample is polycrystalline and the small Co/CoO particles are island-like. The shape of those Co atomic clusters is irregular as shown in Fig. 1(a) and (b), which means that the interface between the FM Co core and the AFM CoO shell is rough. Obviously, the average distance between Co/CoO particles is larger for CCMO1 than for CCMO2.

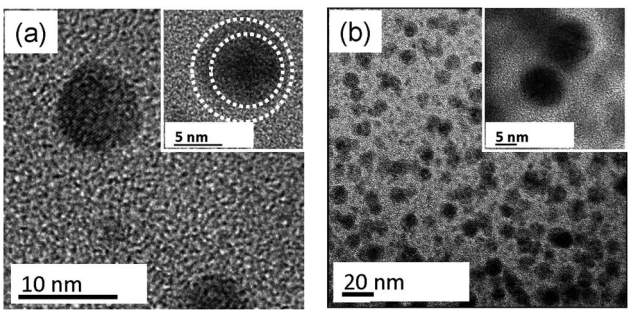

Fig. 1 Transmission electron micrographs (TEM) showing the size and morphology of the CCMO1 (a) and the CCMO2 (b) sample, respectively, revealing the Co/CoO core–shell particles embedded in a MgO matrix.

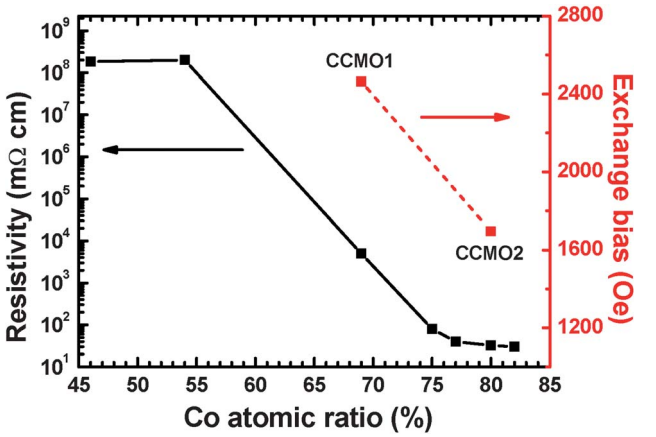

Fig. 2 Resistivity (black squares) as a function of the Co atomic composition ratio at room temperature. The red squares denote the exchange bias field H_E of the CCMO1 and CCMO2 samples at 2 K.

In Fig. 2, we show the room temperature resistivity data as a function of the Co atomic composition ratio. The resistivity drops by about 7 orders of magnitude from 55% to 80% Co atomic ratio. There is a distinct percolation threshold around 69% Co atomic ratio (*i.e.*, for CCMO1) as clearly shown in Fig. 2. We can explain the sharp drop in resistivity as follows: When the Co atomic ratio is less than 69%, the Co/CoO particles are well separated as shown in Fig. 1 and the electron hopping between them is small, the samples thus exhibiting insulating properties. When increasing the Co content, the hopping between core/shell particles becomes possible and the resistance decreases. Although the CCMO1 sample with 69% Co atomic ratio is located at the critical percolation threshold, it still consists of magnetically and electrically well-isolated Co/CoO nanoparticles, whereas the CCMO2 sample has metallic properties, since the electron hopping between core/shell particles is possible.

SQUID magnetization measurements on the CCMO1 sample at 2 K in a magnetic field up to $\mu_0 H = \pm 5$ T are presented in Fig. 3(a). The hysteresis loop for zero-field cooling (ZFC, black line) of the CCMO1 sample is symmetric and thus without EB. On the other hand, the hysteresis loop of the same CCMO1 sample with field cooling in a 5 kOe magnetic field (FC, red line) exhibits a clear asymmetry as compared with the ZFC data, yielding a large H_E of about 2460 Oe and a coercive field of 6200 Oe. We also show the magnetization curves of the CCMO1 sample for various cooling fields in Fig. 4. We find that the exchange-biased hysteresis loops exhibit a considerable positive vertical shift along the magnetization axis for cooling fields from 1 to 50 kOe (see the inset in Fig. 4). As can be seen from Fig. 4, H_E only slightly increases for low cooling fields and stays constant thereafter. Thus, we conclude that the coupling between the pinned uncompensated spins of the CoO shell and the spins of the FM core at the CoO/Co interface is presumably ferromagnetic.[15,20] Our results are in contrast to Co/CoO core–shell nanoparticles in an equally non-magnetic Al_2O_3 matrix[5] where neither a high exchange bias nor a high coercive field could be observed. It is well known that the density of

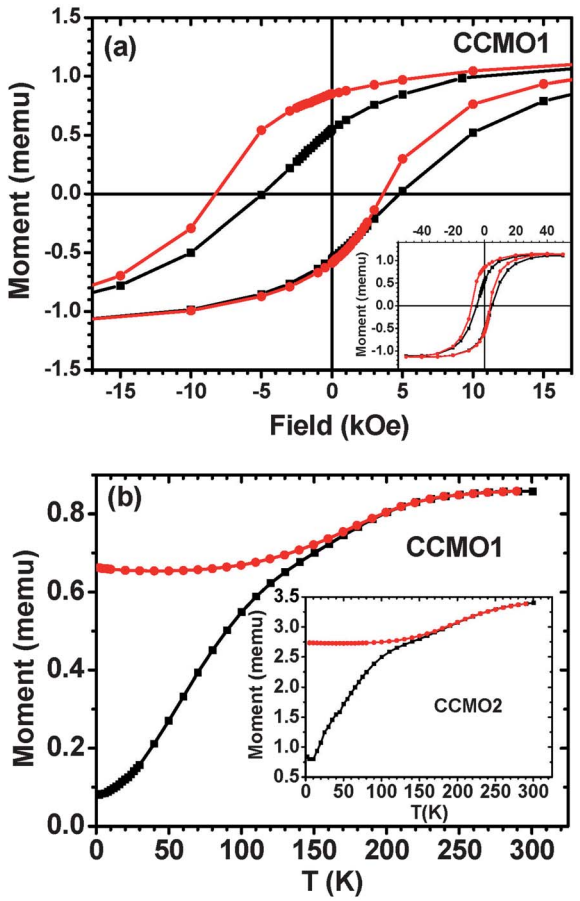

Fig. 3 (a) The ZFC (black lines) and FC (red lines, field cooled at 5 kOe) magnetization curves of the CCMO1 sample at 2 K. The inset shows the whole hysteresis loop. (b) The ZFC (black lines) and FC (red lines, field cooled at 2 kOe) temperature-dependent magnetization curves of sample CCMO1 and CCMO2 (inset) measured at 2 kOe.

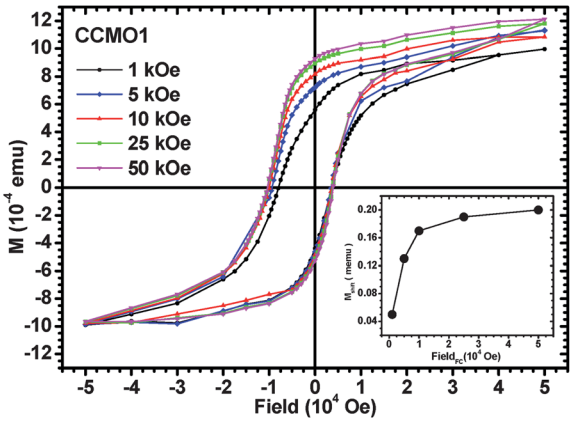

Fig. 4 Field-cooled magnetization curves of the CCMO1 sample taken at 2 K for various cooling fields. The inset shows the dependence of the vertical shift for the magnetization curves along the magnetization axis as a function of the FC cooling field.

nanoparticles does affect H_C and H_E.[21,22] For example, Nogués *et al.*[22] found that H_C and H_E radically increase with increasing coverage (or density) starting from low coverage. To see the effect of nanoparticle density, we have also measured the ZFC and FC magnetization curves of the metallic CCMO2 sample. We find that the increase in nanoparticle density results in a decrease of H_E and H_C to 1696 Oe and 3679 Oe, respectively. We believe that the observed decrease is due to the fact that the CCMO2/CCMO1 samples have a Co atomic ratio above/below the percolation threshold which is concomitant with the increase in particle density. For nanoparticle systems, the superparamagnetic blocking temperature (T_B) is given by the maximum in the ZFC magnetization curve.[23] For CCMO1, the T_B is above 250 K as shown in Fig. 3(b). Since the particle density of CCMO2 is clearly larger than that of CCMO1, the Co atomic ratio of CCMO2 is above the percolation threshold. Consequently, the CCMO2 sample has a considerably larger T_B. The fact that the absolute value of T_B for both samples is unexpectedly high – taking into account the small absolute size of the nanoparticles – can be explained by either the above nanoparticle density or stabilization of the Co FM *via* the CoO AFM.

The lattice structures of the nonmagnetic MgO matrix and the antiferromagnetic CoO shell are very similar.[27] Thus, the non-magnetic Mg atoms are good substituents for Co atoms in the CoO shell. We expect that diluting the Co atoms in the CoO shell with Mg causes the rising of the uncompensated Co spin density at the AFM CoO surface in the same way as reported in the case of multilayered films.[24,25] We list our results in Table 1; for comparison, we also give the results for Co nanoparticles embedded in different matrices.[28,29] Although H_E depends on the core diameter, shell thickness, nanoparticle density, and thus the very details of the sample under consideration, we can still derive a trend where H_E has a decreasing tendency with increasing mismatch between the matrix and CoO crystal lattice parameters. Therefore, the lattice parameter of a (nonmagnetic) matrix material plays an important role in the appearance of the EB in the present Co/CoO–MgO system. Other factors may influence H_E in the Co/CoO–MgO granular film such as the aforementioned interface roughness between the FM core and the AFM shell as well as the particle size in our granular films (being of the order of 5 nm as shown in Fig. 1) as it is known that in that context H_E is inversely proportional to the particle size.[13]

According to the uncompensated spin mechanism, a large H_E should be associated with a large number of pinned uncompensated spins,[15] while a large H_C should be related – among others – to the rotatable uncompensated spins in the AFM CoO shell. The latter is expected to be detectable by soft X-ray magnetic circular dichroism (XMCD) at the Co-$L_{2,3}$ edges, which is an extremely sensitive and element-specific probe for

Table 1 Comparison of H_E and CoO versus matrix material lattice parameter mismatch of Co/CoO core–shell particles

Matrix	Mismatch	H_E(kOe)	Ref.
Al_2O_3	42.6%	0	28
Cr_2O_3	15.7%	0.006	28
SiO_2	14.7%	0.55	29
NiO	1.4%	1.87	29
MgO	1.1%	2.46	This paper

the local environment of the Co ions.[30,31] It is worth mentioning that XMCD had already been used in several core/shell nanoparticle systems.[32–35,46] Thus, we believe that this spectroscopic technique is probably the most appropriate tool to distinguish between the FM signal originating from the nominally AFM CoO shell and the FM signal originating from the Co metal particles, as well as to confirm the existence of rotatable uncompensated spins within the AFM CoO shell.

Fig. 5(a) depicts the Co-$L_{2,3}$ spectra of sample CCMO1 taken using circularly polarized light with the photon spin parallel (μ^+ – red line) and antiparallel (μ^- – black line) with respect to the external magnetic field. The difference spectrum $\Delta\mu = \mu^+ - \mu^-$ (*i.e.*, the XMCD spectrum – blue line) is also shown in Fig. 5(a). The sharp multiplet structures which are observed in the μ^+ and μ^- spectra are very similar to those of CoO,[36] indicating the existence of divalent Co^{2+} (*i.e.*, CoO) in this material. Note the important finding that the XMCD spectrum of the CCMO1 sample has a multiplet spectral structure. The line shape of the XMCD spectrum of CCMO1 is very similar to that found in $LaCo_{0.5}Mn_{0.5}O_3$,[31] in which the Co ions have a divalent state and octahedral local crystal field symmetry. This observation indicates unambiguously that the CoO shell contributes to the XMCD signal and thus gives evidence for FM within the CoO shell due to the existence of rotatable uncompensated spins.[26] A paramagnetic signal for Co^{2+} as reported in other studies at the given elevated sample temperature of 80 K can be ruled out since it would not yield a dichroism with the observed large size (but rather a typical dichroism of 0.6% for a paramagnetic $^4F_{9/2}$ Co^{2+} ion system at 80 K). The observed XMCD signal from the CoO shell in the Co/CoO–MgO system is quite surprising when considering the enormous research effort spent in the field of spectroscopy on dilute FM in nonmagnetic semiconductors and insulators during the past decade, such as 3d TM ions doped into ZnO,[37,42] TiO_2,[38,39,41] and $BaTiO_3$.[40] We can also experimentally rule out the canted AFM scenario since an inversion of the magnetic field together with an inversion of the photon spin did result in the same sign of the XMCD signal.

Now we turn our attention to the CCMO2 sample with a Co atomic composition ratio (80%) above the percolation threshold. In Fig. 5(b), we present the absorption spectra μ^+ and μ^- as well as the XMCD spectrum of CCMO2. Although the sharp multiplet spectral structures are still clearly visible in the μ^+ and μ^- spectra, the multiplet structure in the XMCD spectrum almost disappears. More precisely, one can see that the spectral line shape of the XMCD spectrum is nearly identical to that of Co metal as shown in Fig. 6(f) (magenta line). Here, the μ^+ and μ^- XMCD spectra of Co metal were measured under the same experimental conditions and the overall spectral features are the same as measured using a transmission absorption geometry by Chen *et al.*[43]

From the above observation, we can conclude that the sharp multiplet spectral features in the μ^+ and μ^- absorption spectra of the CCMO2 sample mostly originate from the AFM CoO shell, whereas the spectral structures in the XMCD spectrum with a spectral shape typical for Co metal essentially originate from the Co metal atoms in the core clusters. This is exactly the same observation as in the case of Co clusters doped into TiO_2.[39,41] The magnitude of the XMCD signal is reduced from 7.2% to 4.6% when going from Fig. 5(a) and (b) as the CoO shell does not contribute to the XMCD signal in the CCMO2 sample. For such a large Co content, the size of H_E is close to the value of high-density Co/CoO clusters on CoO thin films.[29,44]

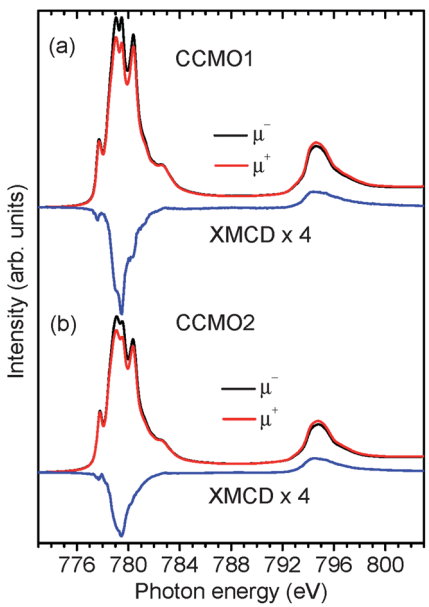

Fig. 5 Co-$L_{2,3}$ XMCD spectra of (a) sample CCMO1 and (b) sample CCMO2 measured at 80 K under a 5 T magnetic field.

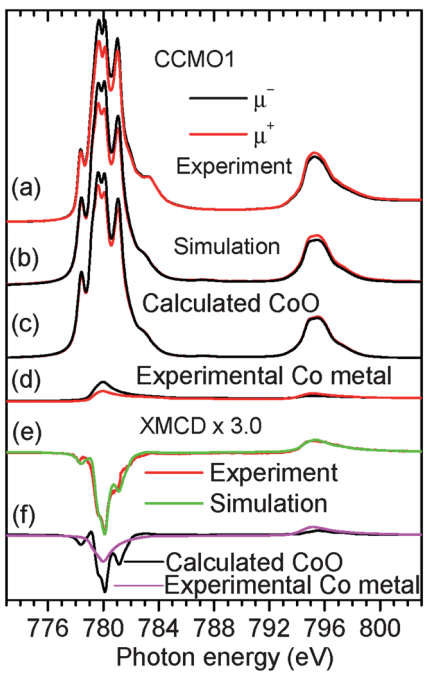

Fig. 6 (a) Experimental μ^+ and μ^- spectra of CCMO1. (b) Simulated μ^+ and μ^- spectra by a superposition of the calculated data for CoO shown in (c) and the experimental data for Co metal shown in (d). (e) Comparison of the experimental XMCD spectrum of CCMO1 and the simulated XMCD spectrum by a superposition of the calculated XMCD from the CoO shell (black line shown in (f)) and experimental Co metal XMCD (magenta line shown in (f)).

In order to estimate the amount of the CoO contribution to XMCD spectra for the CCMO1 sample, we have calculated the multiplet spectrum of the CoO shell using full multiplet calculations including crystal field interactions and covalence. We can simply simulate the experimental spectra of the CCMO1 sample by superposing the calculated spectra for CoO (Fig. 6(c)) and the experimental Co metal spectra (μ^+ (red line) and μ^- (black line)) in Fig. 6(d). In our calculations we use similar parameters as those used for CoO[43] ($U_{dd} = 6.5$ eV, $U_{cd} = 7.7$ eV, $\Delta = 6.5$ eV, $pd\sigma = -1.2$ eV, Slater integrals reduced by 75% from atomic Hartree–Fock values). The simulated μ^+ and μ^- spectra from such a superposition presented in Fig. 6(b) nicely reproduce the experimental spectra given in Fig. 6(a).

Fig. 6(e) also shows the good agreement between the experimental (red line) and the simulated (green line) XMCD spectra. The latter results from a superposition of the calculated XMCD spectrum for the CoO shell (black line shown in (f)) and the experimental XMCD spectrum from Co metal (magenta line shown in (f)). From the above simulation we can estimate that about 70% of the XMCD spectrum is contributed by the CoO shell. However, this does not demonstrate that the CoO shell really contributes 70% of the ordered FM moment, since the effective electron escape depth in our total electron yield XAS spectrum is only a few nm. Our theoretical simulations thus further confirm that the FM signal indeed stems from the CoO shell. This also demonstrates that the XMCD spectrum at the Co-$L_{2,3}$ edges as measured by the total electron yield is the ideal technique for determining the origin of magnetic properties in core–shell nanoparticles.[46]

It is well-known that the magnetic hysteresis loops measured by XMCD at the transition metal L-edges can provide element- and local environment-specific information on the uncompensated spins.[15,46,47] The height of the hysteresis loop is related to the amount of rotatable uncompensated spins. Using different 3d transition metal elements for AFM and FM materials it was found that both FM and AFM sites at the interface can contribute to the height of the hysteresis loop, namely *via* these rotatable uncompensated spins.[47] On the other hand, the vertical shift of the hysteresis loop is related to the amount of pinned interfacial uncompensated spins.[15] Considering that in our Co/CoO systems both the FM core and the AFM shell consist of the same 3d TM element – Co ions – the vertical shift of either the SQUID hysteresis loop (see Fig. 4) or the XMCD hysteresis loop represents the same physical information on the pinned uncompensated spin.[34,46]

Finally, using the XMCD sum rules[48,49] we have derived the ratio m_{orb}/m_{spin} of the Co^{2+} orbital over the spin magnetic moment from the XMCD spectra shown in Fig. 5 that yield a value of 0.24 and 0.17 for CCMO1 and CCMO2, respectively. As mentioned before and as compared to the corresponding figures of 0.57 and 0.095 for CoO[45] and metallic Co,[43] respectively, the large magnetic isotropy of the Co^{2+} ions in these nanoparticle systems is obvious.

4 Conclusion

In summary, a series of nanostructured Co/CoO–MgO thin films were deposited on Si(100) substrates using magnetron sputtering, exhibiting small isolated ferromagnetic Co particles covered with a CoO shell and embedded in a MgO matrix. A distinct conduction percolation threshold with a sharp resistivity decrease around 69% Co atomic ratio has been found. A large exchange bias field ($H_E \approx 2460$ Oe) and coercive field ($H_C \approx 6200$ Oe) were obtained just below this critical percolation threshold. X-ray absorption magnetic circular dichroism at the Co-$L_{2,3}$ edges shows a clear ferromagnetic signal originating from the nominally antiferromagnetic CoO shell. Our work corroborates the uncompensated spin model based on pinned uncompensated spins as well as rotatable uncompensated spins being responsible for the exchange bias and the coercive field, respectively. The observed FM XMCD signal from nominally AFM CoO shells clearly demonstrates the existence of the latter rotatable uncompensated spins.

Acknowledgements

XMCD experiments were performed at the BL29 Boreas beamline at the ALBA Synchrotron Light Facility with the collaboration of ALBA staff. The work was supported by the National Key Project for Basic Research of China (Grant no. 2012CB932304), NSFC (no. U1232210, 91122035, 11174124, and 11204124.) and PAPD.

Notes and references

1 W. H. Meiklejohn and C. P. Bean, *Phys. Rev.*, 1956, **102**, 1413.
2 B. Dieny, V. S. Speriosu, S. Metin, S. Parkin, B. A. Gurney, P. Baumgart and D. R. Wilhoit, *J. Appl. Phys.*, 1991, **69**, 4774.
3 B. Dieny, V. S. Speriosu, S. S. P. Parkin, B. A. Gurney, D. R. Wilhoit and D. Mauri, *Phys. Rev. B: Condens. Matter Mater. Phys.*, 1991, **43**, 1297.
4 B. Dieny, *J. Magn. Magn. Mater.*, 1994, **136**, 335.
5 V. Skumryev, S. Stoyanov, Y. Zhang, G. Hadjipanayis, D. Givord and J. Nogués, *Nature*, 2003, **423**, 850.
6 J. Nogués, J. Sort, V. Langlais, V. Skumryev, S. Suriñach, J. S. Muñoz and M. D. Baró, *Phys. Rep.*, 2005, **422**, 65.
7 V. Laukhin, V. Skumryev, X. Martí, D. Hrabovsky, F. Sánchez, M. V. García-Cuenca, C. Ferrater, M. Varela, U. Lüders, J. F. Bobo and J. Fontcuberta, *Phys. Rev. Lett.*, 2006, **97**, 227201.
8 M. Ali, P. Adie, C. H. Marrows, D. Greig, B. J. Hickey and R. L. Stamps, *Nat. Mater.*, 2007, **6**, 70.
9 H. Béa, M. Bibes, F. Ott, B. Dupé, X. H. Zhu, S. Petit, S. Fusil, C. Deranlot, K. Bouzehouane and A. Barthélémy, *Phys. Rev. Lett.*, 2008, **100**, 017204.
10 J. de la Venta, M. Erekhinsky, S. Wang, K. G. West, R. Morales and I. K. Schuller, *Phys. Rev. B: Condens. Matter Mater. Phys.*, 2012, **85**, 134447.
11 E. Lage, C. Kirchhof, V. Hrkac, L. Kienle, R. Jahns, R. Knöchel, E. Quandt and D. Meyners, *Nat. Mater.*, 2012, **11**, 523.
12 S. Laureti, S. Y. Suck, H. Haas, E. Prestat, O. Bourgeois and D. Givord, *Phys. Rev. Lett.*, 2012, **108**, 077205.
13 K. Takano, R. H. Kodama, A. E. Berkowitz, W. Cao and G. Thomas, *Phys. Rev. Lett.*, 1997, **79**, 6.

14 H. Ohldag, T. J. Regan, J. Stöhr, A. Scholl, F. Nolting, J. Lüning, C. Stamm, S. Anders and R. L. White, *Phys. Rev. Lett.*, 2001, **87**, 247201.
15 H. Ohldag, A. Scholl, F. Nolting, E. Arenholz, S. Maat, A. T. Young, M. Carey and J. Stöhr, *Phys. Rev. Lett.*, 2003, **91**, 017203.
16 Y. Ijiri, J. A. Borchers, R. W. Erwin, S. H. Lee, P. J. van der Zaag and R. M. Wolf, *Phys. Rev. Lett.*, 1998, **80**, 608.
17 W. J. Antel Jr, F. Perjeru and G. R. Harp, *Phys. Rev. Lett.*, 1999, **83**, 1439.
18 R. F. L. Evans, D. Bate, R. W. Chantrell, R. Yanes and O. Chubykalo-Fesenko, *Phys. Rev. B: Condens. Matter Mater. Phys.*, 2011, **84**, 92404.
19 C. Dufour, M. R. Fitzsimmons, J. A. Borchers, M. Laver, K. L. Krycka, K. Dumesnil, S. M. Watson, W. C. Chen, J. Won and S. Singh, *Phys. Rev. B: Condens. Matter Mater. Phys.*, 2011, **84**, 064420.
20 J. Nogués, C. Leighton and I. K. Schuller, *Phys. Rev. B: Condens. Matter Mater. Phys.*, 2000, **61**, 1315.
21 G. Margaris, K. N. Trohidou and J. Nogués, *Adv. Mater.*, 2012, **24**, 4331.
22 J. Nogués, V. Skumryev, J. Sort, S. Stoyanov and D. Givord, *Phys. Rev. Lett.*, 2006, **97**, 157203.
23 M. Knobel, W. C. Nunes, L. M. Socolovsky, E. De Biasi, J. M. Vargas and J. C. Denardin, *J. Nanosci. Nanotechnol.*, 2008, **8**, 2836.
24 J.-I. Hong, T. Leo, D. J. Smithand and A. E. Berkowitz, *Phys. Rev. Lett.*, 2006, **96**, 117204.
25 J. Keller, P. Miltényi, B. Beschoten, G. Güntherodt, U. Nowak and K. D. Usadel, *Phys. Rev. B: Condens. Matter Mater. Phys.*, 2002, **66**, 014431.
26 S. Urazhdin and C. L. Chien, *Phys. Rev. B: Condens. Matter Mater. Phys.*, 2005, **71**, 220410.
27 T. Leo, J.-I. Hong, A. E. Berkowitz and D. J. Smith, *J. Appl. Phys.*, 2007, **102**, 123904.
28 D. Tobia, E. Winkler, R. D. Zysler, M. Granada, H. E. Troiani and D. Fiorani, *J. Appl. Phys.*, 2009, **106**, 103920.
29 C. Portemont, R. Morel, A. Brenac and L. Notin, *J. Appl. Phys.*, 2006, **100**, 033907.
30 J. A. Moyer, C. A. F. Vaz, D. A. Arena, D. Kumah, E. Negusse and V. E. Henrich, *Phys. Rev. B: Condens. Matter Mater. Phys.*, 2011, **84**, 054447.
31 T. Burnus, Z. Hu, H. H. Hsieh, V. L. J. Joly, P. A. Joy, M. W. Haverkort, H. Wu, A. Tanaka, H.-J. Lin, C. T. Chen and L. H. Tjeng, *Phys. Rev. B: Condens. Matter Mater. Phys.*, 2008, 77, 125124.
32 A. Lopez-Ortega, M. Estrader, G. Salazar-Alvarez, S. Estrade, I. V. Golosovsky, R. K. Dumas, D. J. Keavney, M. Vasilakaki, K. N. Trohidou, J. Sort, F. Peiro, S. Surinach, M. D. Baro and J. Nogues, *Nanoscale*, 2012, **4**, 5138.
33 Y. Prado, M.-A. Arrio, F. Volatron, E. Otero, C. Cartier dit Moulin, P. Sainctavit, L. Catala and T. Mallah, *Chem.–Eur. J.*, 2013, **19**, 6685.
34 D. Nolle, E. Goering, T. Tietze, G. Schütz, A. Figuerola and L. Manna, *New J. Phys.*, 2009, **11**, 033034.
35 U. Wiedwald, M. Spasova, E. L. Salabas, M. Ulmeanu and M. Farle, *Phys. Rev. B: Condens. Matter Mater. Phys.*, 2003, **68**, 064424.
36 S. I. Csiszar, M. W. Haverkort, Z. Hu, A. Tanaka, H. H. Hsieh, H. J. Lin, C. T. Chen, T. Hibma and L. H. Tjeng, *Phys. Rev. Lett.*, 2005, **95**, 187205.
37 T. Tietze, M. Gacic, G. Schütz, G. Jakob, S. Brück and E. Goering, *New J. Phys.*, 2008, **10**, 055009.
38 Y. Matsumoto, M. Murakami, T. Shomo, T. Hasegawa, T. Fukumara, M. Kawasaki, P. Ahmet, T. Chikyov, S. Koshihara and H. Koinuma, *Science*, 2001, **291**, 854.
39 T. Ohtsuki, A. Chainani, R. Eguchi, M. Matsunami, Y. Takata, M. Taguchi, Y. Nishino, K. Tamasaku, M. Yabashi, T. Ishikawa, M. Oura, Y. Senba, H. Ohashi and S. Shin, *Phys. Rev. Lett.*, 2011, **106**, 047602.
40 T. Chakraborty, S. Ray and M. Itoh, *Phys. Rev. B: Condens. Matter Mater. Phys.*, 2011, **83**, 144407.
41 J. Y. Kim, J. H. Park, B. G. Park, H. J. Noh, S. J. Oh, J. S. Yang, D. H. Kim, S. D. Bu, T. W. Noh, H. J. Lin, H. H. Hsieh and C. T. Chen, *Phys. Rev. Lett.*, 2003, **90**, 017401.
42 B. B. Straumal, A. A. Mazilkin, S. G. Protasova, A. A. Myatiev, P. B. Straumal, G. Schütz, P. A. van Aken, E. Goering and B. Baretzky, *Phys. Rev. B: Condens. Matter Mater. Phys.*, 2009, **79**, 205206.
43 C. T. Chen, Y. U. Idzerda, H.-J. Lin, N. V. Smith, G. Meigs, E. Chaban, G. H. Ho, E. Pellegrin and F. Sette, *Phys. Rev. Lett.*, 1995, **75**, 152.
44 D. L. Peng, K. Sumiyama, T. Hihara, S. Yamamuro and T. J. Konno, *Phys. Rev. B: Condens. Matter Mater. Phys.*, 2000, **61**, 3103.
45 G. Ghiringhelli, L. H. Tjeng, A. Tanaka, O. Tjernberg, T. Mizokawa, J. L. de Boer and N. B. Brookes, *Phys. Rev. B: Condens. Matter Mater. Phys.*, 2002, **66**, 075101.
46 F. Jiménez-Villacorta, C. Prieto, Y. Huttel, N. D. Telling and G. van der Laan, *Phys. Rev. B: Condens. Matter Mater. Phys.*, 2011, **84**, 172404.
47 J. Nogués, S. Stepanow, A. Bollero, J. Sort, B. Dieny, F. Nolting and P. Gambardella, *Appl. Phys. Lett.*, 2009, **95**, 152515.
48 B. T. Thole, P. Carra, F. Sette and G. van der Laan, *Phys. Rev. Lett.*, 1992, **68**, 1943.
49 P. Carra, B. T. Thole, M. Altarelli and X. Wang, *Phys. Rev. Lett.*, 1993, **70**, 694.